HHS Public Access

Author manuscript

Cell Rep. Author manuscript; available in PMC 2017 June 26.

Published in final edited form as:

Cell Rep. 2017 April 18; 19(3): 521–531. doi:10.1016/j.celrep.2017.03.061.

Diversity in Excitation-Inhibition Mismatch Underlies Local Functional Heterogeneity in the Rat Anterior Auditory Field

Can Tao[1,3], **Guangwei Zhang**[1,3], **Chang Zhou**[1], **Lijuan Wang**[1], **Sumei Yan**[1], **Huizhong Whit Tao**[2], **Li I. Zhang**[2], **Yi Zhou**[1,*], and **Ying Xiong**[1,4,*]

[1]Department of Neurobiology, Chongqing Key Laboratory of Neurobiology, Third Military Medical University, Chongqing 400038, China

[2]Zilkha Neurogenetic Institute, Keck School of Medicine, University of Southern California, Los Angeles, CA 90033, USA

Summary

Cortical neurons are heterogeneous in their functional properties. This heterogeneity is fundamental for the processing of different features of sensory information. However, functional diversity within a local group of neurons is poorly understood. Here, we demonstrate that neighboring cortical neurons in layer 5 but not those of layer 4 of the rat anterior auditory field (AAF) exhibited a surprisingly high level of diversity in tonal receptive fields. In vivo whole-cell voltage-clamp recordings revealed that the diversity of frequency representation was due to a spectral mismatch between synaptic excitation and inhibition to varying degrees. The spectral distribution of excitation was skewed at different levels, while inhibition was homogeneous and non-skewed, similar to the summed spiking activity of local neuronal ensembles, which further enhanced diversity. Our results indicate that AAF in the auditory cortex is involved in processing auditory information in a highly refined manner that is important for complex pattern recognition.

In Brief

Tao et al. look at how local heterogeneity is generated in the anterior auditory field using an in vivo electrophysiological approach and find that a diverse excitation-inhibition imbalance generates functional heterogeneity in L5 of the anterior auditory field.

[*]Correspondence: zhouyisjtu@gmail.com (Y. Z.), xiongying2001@163.com (Y. X.).

[3]Co-first author

[4]Lead Contact

Author Contributions

L.I.Z., Y.Z. and Y.X. designed the experiments and supervised the work. C.T. and G.Z. performed the electrophysiological experiments. C.T. and G.Z. analyzed the data and prepared the figures. C.Z., L.W. and S.Y. performed the histological experiments. H.W.T., L.I.Z., Y.Z. and Y.X. prepared the manuscript with input from C.T. and G.Z.. All authors discussed the results and commented on the manuscript.

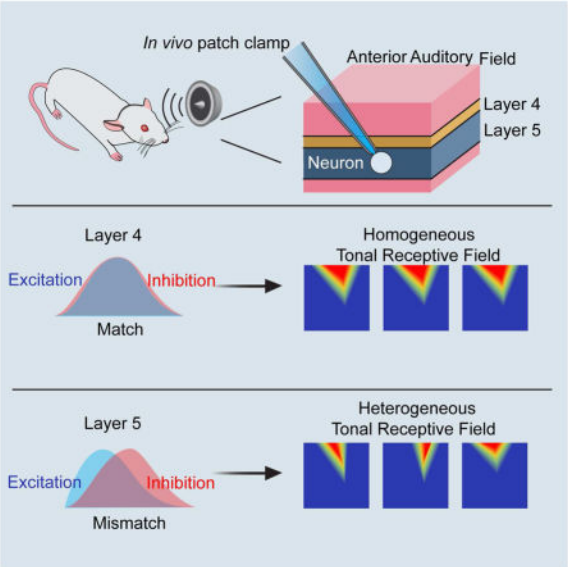

Keywords

auditory cortical field; excitation/inhibition balance; synaptic circuit mechanism; frequency and intensity tuning

Introduction

One prominent feature of auditory cortical neurons is their tuning for sound frequency (Read et al., 2002; Schreiner et al., 2000). The tuning of single neurons or neuronal ensembles can be quantified by measuring the tonal receptive field (TRF) of neuronal responses to pure tones of different frequencies and intensities (Kanold et al., 2014; Rothschild and Mizrahi, 2015). While overall there is a refined representation of frequency along a tonotopic gradient (Guo et al., 2012; Zhang et al., 2001), neurons in the same frequency band exhibit heterogeneity in terms of best frequency (BF) and tuning bandwidth (Schreiner and Sutter, 1992). Such diversity has also been reported for neurons across different laminar locations within the same cortical column (Abeles and Goldstein, 1970; Sakata and Harris, 2009; Sugimoto et al., 1997; Wallace and Palmer, 2008). Recent two-photon calcium imaging and visually guided loose-patch recording studies (Bandyopadhyay et al., 2010; Maor et al., 2016; Rothschild et al., 2010; Winkowski and Kanold, 2013) have reported that BF of even nearby neurons can be quite heterogeneous, and that such local heterogeneity is much more pronounced in superficial than in middle layers (Winkowski and Kanold, 2013). The abovementioned studies were mostly carried out in the primary visual cortex (A1). By differentiating single units from multi-unit recordings, local functional diversity has been shown to be present in other auditory cortical areas, such as the anterior auditory field (AAF) (South and Weinberger, 1995), which has a mirrored tonotopic gradient with A1 (Lomber and Malhotra, 2008; Merzenich et al., 1975), and data from a reversible cooling study in the cat have suggested that the AAF plays an important role in complex pattern discrimination tasks (Lomber and Malhotra, 2008). In addition to the auditory cortex,

varying degrees of local functional diversity have also been observed in other sensory cortices of rodents (Kerlin et al., 2010; Ohki et al., 2005; Smith and Hausser, 2010; Stettler and Axel, 2009).

Neurons in different cortical layers exhibit different response properties, and this characteristic has been thought to reflect the differential roles that these layers play in auditory information processing (Li et al., 2014; Sun et al., 2013; Wu et al., 2011; Zhou et al., 2010). Recent in vivo whole-cell recording studies have examined the synaptic mechanisms underlying laminar-specific response properties (Li et al., 2014; Sun et al., 2013; Zhou et al., 2010), which are characterized by distinct spectrotemporal interplays of excitation and inhibition (Wu et al., 2011). For example, in L4 of the primary auditory cortex, spectrally balanced excitation and feedforward inhibition allow for a faithful representation of auditory information relayed from the thalamus (Sun et al., 2010; Wehr and Zador, 2003; Zhang et al., 2003; Zhou et al., 2015), while in L6, a presumptive disynaptic excitatory feedforward circuit can result in an earlier arrival of inhibition than excitation, which suppresses the tone responses of a subset of L6 projection neurons (Zhou et al., 2010). In short, various relationships between sound-evoked excitation and inhibition, in terms of relative spectral tuning, temporal order of activation and amplitude ratio, result in laminar-dependent processing properties, and these differences are attributed to differences in the construction of synaptic circuits in various lamina (Wu et al., 2011).

Compared with differential laminar processing, our understanding of local functional heterogeneity remains very limited. First, the strong local heterogeneity of BF in A1 superficial layers was reported in anesthetized animals using calcium imaging with chemical sensors (Bandyopadhyay et al., 2010; Rothschild et al., 2010; Winkowski and Kanold, 2013) but was much less apparent in awake animals with genetically encoded calcium sensors (Issa et al., 2014; Kato et al., 2015), as evidenced by the relatively small and smooth change in BF across neighboring neurons. One possibility is that heterogeneity may exist at a relatively local scale in A1 of awake animals (Kanold et al., 2014). Nevertheless, an important question is how functional heterogeneity can be generated in an apparently homogeneous group of neurons, i.e., excitatory projection neurons that are embedded in the same local circuit. Thus, this is a different issue from that of the generation of laminar diversity.

In the present study of rat AAF, we found that the TRF profiles of adjacent neurons in L4 were relatively homogeneous, whereas those of adjacent neurons in L5 showed remarkable diversity. The different levels of heterogeneity in these two layers of AAF provide a good model for probing the synaptic mechanisms underlying local functional diversity. By performing sequential in vivo whole-cell current clamp and voltage clamp recordings, we found that AAF L5 neurons received excitatory and inhibitory inputs that were spectrally mismatched to varying degrees, as manifested by a differentially skewed spectral distribution of excitation together with a homogeneously non-skewed distribution of inhibition. On the other hand, neurons in L4 mostly received well-matched excitation and inhibition. The degree of the mismatch between excitation and inhibition was highly correlated with the tuning diversity of spike responses. With these results, we have described a simple yet effective mechanism to account for the generation of local functional diversity in AAF L5.

Results

Diverse tuning patterns in L5 of awake rat auditory cortex

We first performed multiunit recordings to map the auditory cortex in awake, head-fixed rats (Figure 1A, see Experimental Procedures). After locating the A1 and AAF based on their mirrored tonotopic gradients, we injected a retrograde tracer, cholera toxin subunit B (CTb), into functionally localized low-frequency regions of A1 and AAF (Figure 1A, see Experimental Procedures). We found that A1 primarily received input from the ventral division of the medial geniculate body (MGv), while AAF received strong input from outside the MG, such as the posterior complex (Po) of the thalamus (Figure 1A and Figure S1), which is consistent with previous reports (Ehret and Romand, 1997; Morel and Imig, 1987). To assay local functional diversity, we examined how the functional similarity among neurons within a local ensemble by comparing the TRF profiles of single neurons with those of multiunit activity (MUA), which reflects the summed activity of the local neuronal population. For this purpose, we first mapped the frequency-intensity TRF of a cortical site using a tungsten electrode and then switched to a glass pipette to make single-cell loose-patch recordings at roughly the same location (Figure S2, see Experimental Procedures). In the frequency-intensity space, the preferred frequency-intensity combination (which evoked the highest spike rate) of the neuronal ensemble (MUA) was set as the origin. The preferred frequency-intensity combination of a single neuron was then depicted by a vector, which illustrates its deviation (ΔFrequency and ΔIntensity) from the MUA (Figure 1B, right bottom). We found that the preferred frequency-intensity combinations of L4 neurons closely resembled those of their local neuronal ensembles, whereas for L5 neurons, the preferred frequency-intensity combination could be quite different from that of their local ensembles, suggesting a higher level of local functional diversity in L5 (see below). Consistent with the mismatch of TRF profiles between single neurons and the MUA, adjacent L5 cells (<120 μm in distance, see Experimental Procedures) exhibited a large variation in the shape and subtle location of their TRFs (Figure 1D), whereas adjacent L4 neurons exhibited very similar TRFs (Figure 1C). The local heterogeneity in L5 is further illustrated by the much smaller overlap between the TRFs of adjacent cells (Figure 1F) compared with that of the L4 TRFs (Figure 1E). The TRFs of adjacent L5 cells, including classic V-shaped and irregular, non-V-shaped TRFs (Sadagopan and Wang, 2008; Wu et al., 2006), were all enclosed by the V-shaped TRF of MUA (Figure 1F and Figure S3), suggesting that the TRF profiles of L5 cells are not completely disordered. Interestingly, the V-shaped TRF of MUA can be replicated by averaging the TRFs of local single cells, whether they have V-shaped TRFs or not (Figure S3). Similar local functional diversity was also observed in L5 of anesthetized rats (Figure 1E and 1F, bottom panel).

By aligning the vectors of different neurons, it becomes clear that neurons in L4 (n = 10) had similar frequency-intensity preferences to those of their local neuronal ensembles, whereas L5 neurons (n = 16) had largely different and diverse preferences compared with those of their local ensembles (Figure 2A, left). Similar observations were made in anesthetized rats (Figure 2A, right). Overall, L5 neurons exhibited a significantly larger deviation in frequency and intensity preferences from the local ensemble than L4 cells (**, $p < 0.01$,

Welch *t* test, Figure 2B and 2C). The levels of deviation were found to be comparable in awake and anesthetized animals ($p > 0.05$, *t* test, Figure 2B, 2C).

In addition to frequency and intensity preferences, we also examined the size of the TRF, which was defined as the sum of bandwidths at all testing intensities. We calculated the ratio of TRF sizes between a single neuron (SUA) and its local neuronal ensemble, which ranges between 0 and 1 and can be used as a similarity index. L4 neurons exhibited a narrow distribution of size ratios (Figure 2D). By contrast, L5 neurons showed a much broader distribution; some neurons responded exclusively to a narrow range of frequency-intensity combinations, while others responded in a similar manner to that of MUA (Figure 2E). The average similarity index of L5 neurons (0.57 ± 0.61, awake; 0.63 ± 0.41, anesthetized, shown as the mean ± SD, unless otherwise specified) was significantly lower than that of L4 cells (0.81 ± 0.61, awake; 0.84 ± 0.28, anesthetized, both $p < 0.01$, Welch *t* test). L5 also exhibited a broader distribution of similarity indices ($\sigma = 0.41$ in L5 vs. 0.28 in L4, $p < 0.01$, F-test, Figure 2F). Taken together, these results demonstrate remarkable TRF diversity in L5 but not in L4. This difference between L4 and L5 in both awake and anesthetized conditions provides a good basis for investigating the mechanisms underlying local functional diversity.

Diversity of subthreshold responses in L5

We demonstrated that L5 neurons exhibited a larger deviation in BF from MUA than L4 cells at the intensity level of 60 dB sound pressure level (SPL) (Figure 3A). Focusing on this intensity level, we performed whole-cell current clamp recording to understand the subthreshold mechanisms underlying the frequency tuning diversity of spike responses. Postsynaptic membrane potential (PSP) responses to tones of various frequencies at 60 dB SPL were recorded in L4 (Figure 3B) and L5 (Figure 3C) cells. We compared the frequency tuning of PSP (after filtering out spikes) and MUA by calculating the difference in BF (ΔBF, Figure 3B, 3C, colored arrows). In addition, we compared the center of the frequency response range (determined at a threshold of 3 standard deviations above baseline) between MUA tuning and PSP tuning. While L4 and L5 neurons had similarly small differences in the center of the frequency response range (Figure 3D), L5 neurons exhibited a significantly larger ΔBF than L4 neurons ($p < 0.01$, Welch *t* test, Figure 3E), indicating that their large deviation in BF from MUA cannot be attributed to a shift of the tuning curve as a whole. Instead, the ΔBF was more likely due to a difference between the exquisite shapes of PSP and MUA tuning; while the MUA and L4 PSP tuning curves were more or less symmetrical, the L5 PSP tuning was sometimes highly skewed (Figure 3C, 3F). Overall, the shape of L5 PSP tuning was significantly more diverse than that of MUA and L4 PSP tuning (Figure 3G). For L5 cells, the skewness of PSP tuning was positively correlated with the ΔBF between MUA and PSP (Figure 3H). These results demonstrate that the subthreshold membrane potential response also has a higher level of tuning diversity in L5 than in L4, which can directly explain the diverse frequency preferences of the spike responses of adjacent L5 neurons (Figure 1). However, the synaptic mechanisms that can account for these diverse preferences remain to be explored.

Skewed excitatory tuning primarily contributes to the functional diversity in L5

To further explore synaptic mechanisms, we performed sequential current clamp and voltage clamp recordings to obtain membrane potential changes (output) and excitatory/inhibitory synaptic currents (input) in response to tones of various frequencies from the same neuron. Linear current-voltage (I-V) curves were obtained for the recorded white noise-evoked synaptic currents, suggesting a reasonably good voltage clamp quality (Figure S4). Figures 4A and 4B show two representative cells. We identified the BF for the tuning of PSP, excitation and inhibition in the same recorded cell, as well as that of MUA of its local neuronal ensemble. In L5, BF of synaptic excitation deviated much more than that of synaptic inhibition from MUA (ΔBF: 0.59 ± 0.27 vs 0.17 ± 0.13 octave, $p < 0.01$, Welch *t* test, Figure 4C). By contrast, BF of synaptic inhibition deviated more than that of synaptic excitation from PSP (0.72 ± 0.54 vs. 0.19 ± 0.14 octave, $p < 0.01$, Welch *t* test, Figure 4D). On the other hand, the ΔBF between synaptic response and MUA or PSP was similarly small for excitation and inhibition in L4 (Figure 4C, 4D). These results indicate that the tuning of excitation is more similar to that of PSP, suggesting that the functional property of a neuron is mainly determined by its excitatory input. Therefore, the large difference between BFs of excitation and MUA indicates that the diversity of excitatory tuning is the main reason for the local frequency tuning diversity in L5. On the other hand, the similarity between BFs of inhibition and MUA indicates that inhibition is more homogeneous than excitation. The difference between BFs of inhibition and PSP suggest that inhibition is not the determinant factor for the local frequency tuning diversity.

To further understand the differences in BF, we measured the skewness of PSP, excitation, inhibition and MUA tuning. In L4, these four tuning curves were essentially non-skewed, as shown by the skewness values close to zero (Figure 4E). In L5, PSP and excitatory tuning curves were much more skewed than MUA and inhibition, and the direction of skew was diverse, as shown by both positive and negative skewness values (Figure 4F). The skewness of excitatory tuning was positively correlated with the ΔBF between PSP and MUA (Figure 4G), while the skewness of inhibitory tuning was not (Figure 4H). Moreover, excitation and inhibition mismatched significantly in L5 cells, as indicated by a large difference between their BFs (ΔBF: 0.56 ± 0.38 octave vs 0.17 ± 0.12 octave in L4) (Figure 4I). This mismatch was positively correlated with the ΔBF between PSP and MUA (Figure 4J). Together, these data demonstrate that the differentially skewed excitatory tuning primarily contributes to the diversity of output response.

Inhibition augments the difference in BF between PSP and MUA

Although the ΔBF between PSP and MUA was mainly attributed to the skewed excitatory tuning, it was significantly larger than the δBF between excitation and MUA (Figure 5A). To understand whether inhibition contributes to this difference, we used a conductance-based single-compartment neuron model (see Experimental Procedures) to derive the expected PSP response from the recorded synaptic conductance. We derived PSP based on excitatory input only, as well as on the integration of excitation and inhibition (Figure 5B). In the presence of inhibition, the ΔBF between the derived and recorded PSP was significantly reduced (Figure 5C, 5D), suggesting that inhibition had in fact shifted BF of the output response. We also found that the ΔBF between the derived PSP and MUA was increased in

the presence of inhibition, which then became more similar to the ΔBF between the recorded PSP and MUA (Figure 5E). These results suggest that inhibition augments the difference in BF between PSP and MUA and thus enhances the diversity of BFs in L5 neurons.

Synaptic onset latencies of excitation and inhibition

Finally, we investigated the onset latencies of synaptic excitation and inhibition evoked by BF (Figure 6A). For neurons in L4, the onset latency of inhibition was slightly but significantly longer than that of excitation (9.6 ± 0.4 ms vs. 8.2 ± 0.5 ms) (Figure 6B), consistent with the previous notion in A1 that inhibition (at least the fastest component) in L4 is due to a disynaptic feedforward inhibitory circuit (Zhang et al., 2003). On the other hand, in L5 neurons, the onset latency of inhibition was not different from that of excitation (16.6 ± 0.5 ms vs. 17.1 ± 0.4 ms), and both were several milliseconds longer than their counterparts in L4 (Figure 6C). These results indicate that the excitatory and inhibitory inputs to L5 neurons come from different sources than those to L4 neurons. While L4 neurons likely receive thalamic inputs, the direct inputs to L5 neurons are unlikely to be thalamic, which are different from those to A1 L5 neurons (Intskirveli et al., 2016; Sun et al., 2013; Szymanski et al., 2009). In addition, unlike L4, the inhibitory input to L5 cells may not be accounted for by a disynaptic feedforward inhibitory circuit.

Discussion

By comparing the TRF profile of a single neuron with its nearby cells and its local neuronal ensemble, we have discovered a laminar difference in local functional diversity between L4 and L5 in the anterior auditory field of rat auditory cortex. In addition, we have revealed distinct contributions of different synaptic input components to the remarkable diversity in L5. Excitatory input with diverse tuning asymmetry played a leading role in determining diverse BF, and inhibitory input with relatively uniform tuning symmetry can further enhance the diversity of BFs. Our results demonstrate unprecedented flexible pairing between excitation and inhibition in cortical neurons and demonstrate that the diverse excitation-inhibition mismatch patterns underlie the local tuning diversity.

The laminar difference in local functional diversity between L4 and L5

Previously, laminar differences in local functional diversity have been reported for L4 and supragranular L2/3 in the auditory cortex (Abeles and Goldstein, 1970; Bandyopadhyay et al., 2010; Hromadka et al., 2008; Rothschild et al., 2010; Winkowski and Kanold, 2013). Our result showing that the TRFs of adjacent L4 neurons are relatively homogeneous is consistent with the previous notion that L4 has a low level of local diversity. Together with our findings of remarkable diversity in L5, we suggest that local diversity may be enhanced as information flows from the granular layer to the supra- and infragranular layers (Callaway, 1998). These results are also reminiscent of findings showing that preferred orientations are less biased in L5 and L2/3 compared with those in L4 in the mouse visual cortex (Sun et al., 2016). As the major thalamorecipient layer, L4 receives and amplifies thalamic signals (Li et al., 2013a; Li et al., 2013b; Lien and Scanziani, 2013). On the other hand, L5 is known to be a primary corticofugal layer, at least in the primary sensory cortex. Previous research has suggested that L5 is involved in decision making in sound

discrimination tasks (Znamenskiy and Zador, 2013) and in modulating sound-driven flight behaviors (Xiong et al., 2015). Although the function of the AAF L5 is not yet clear, the result demonstrating that the AAF is important for complex pattern discrimination (Lomber and Malhotra, 2008) raises the possibility that the high level of diversity in the AAF L5 helps the lamina to meet its challenging functional needs.

Excitation-inhibition mismatch in L5

In L4 of A1, relatively balanced synaptic excitation and inhibition were widely observed in that the frequency tuning of excitatory input is similar to that of inhibitory input (Wehr and Zador, 2003; Wu et al., 2008; Zhang et al., 2003). However, in other layers including L5, the interplay between excitation and inhibition can be more complex (Li et al., 2014; Sun et al., 2013; Zhou et al., 2010). For example, in a subset (intrinsic bursting cells) of L5 neurons, inhibition is more narrowly tuned than excitation (Sun et al., 2013). In this study, our results in AAF L4 are consistent with previous results in A1 L4 in that neurons receive essentially balanced excitation and inhibition. In addition, the onset latency of inhibition is slightly longer than that of excitation (Figure 6A, 6B), consistent with a classic disynaptic feedforward inhibitory circuit proposed for L4 cells in A1 (Zhang et al., 2003; Zhou et al., 2010). Similar to that in A1, the tuning relationship between excitation and inhibition also becomes more complex in L5. However, the mismatch between excitation and inhibition in AAF L5 cells is more subtle than that in A1 L5 (Sun et al., 2013); while the inhibitory tuning profile is largely symmetric, the excitatory tuning can be skewed, leading to a mismatch of BF of excitation and inhibition. The excitatory and inhibitory tuning profiles otherwise largely overlap (Figure S5). Furthermore, the onset latency of excitation in L5 cells is much longer than that in L4 cells, and the onset latency of inhibition is not different from excitation (Figure 6C). These results suggest that, different from A1 L5 (Intskirveli et al., 2016; Sun et al., 2013; Szymanski et al., 2009), AAF L5 cells receive excitation only from intracortical sources (e.g., L2/3), and not thalamic sources. Furthermore, the inhibition to L5 cells may arrive in parallel with their feedforward excitation (e.g., intralaminar inhibition from L2/3, see (Jiang et al., 2015; Jiang et al., 2013)), which is different from the disynaptic feedforward inhibition to A1 L5 (Sun et al., 2013).

A proposed model for the mismatch in excitation and inhibition

As our latency analysis suggests that excitatory and inhibitory inputs to AAF L5 cells are all intracortical, here we propose a model for the formation of the observed excitation-inhibition mismatch. In our model (Figure 6D), the presynaptic neurons (both excitatory and inhibitory) of an L5 cell all have symmetric spiking tuning profiles. The distribution of the synaptic weights of the inputs is asymmetric for excitatory connections and symmetric for inhibitory connections. Summing up the weighted synaptic inputs then produces skewed excitatory tuning and non-skewed inhibitory tuning (Figure 6D). By varying the distribution pattern of synaptic weights, this model also explains how the diverse asymmetry of excitation is generated in a group of neurons with the same configuration of circuit connectivity. Previous studies have suggested that excitatory synaptic connections can be modulated in an asymmetric manner through spike-timing dependent plasticity (Engert et al., 2002; Fu et al., 2004; Mehta et al., 2000). On the other hand, spike-timing dependent plasticity of inhibitory synapses often follows different rules from those of excitatory

synapses (Dan and Poo, 2006; Woodin et al., 2003). This difference in plasticity may allow inhibitory connections to have a strength distribution different from excitatory connections onto the same cell (see also (Li et al., 2015)).

Another possibility is that the subcellular spatial distribution of synaptic sites could also contribute to the apparent asymmetric distribution of excitatory synaptic strengths. For example, inputs evoked by tones away from the BF of MUA, when closer to the cell body than those evoked by tones corresponding to the BF of MUA, can give rise to larger responses seen at the soma than the latter. In this case, the synaptic weight seen at the soma can be viewed as an “effective” synaptic weight that reflects the impact of the input on the cell body. We have shown that derived PSP responses from integrating recorded excitation and inhibition have a similar tuning pattern as the PSP responses recorded in the same cell (Figure 5). This result provides strong evidence that the recorded synaptic responses accurately reflect effective synaptic impacts on the soma.

Excitation-inhibition mismatch underlies local heterogeneity

Our results show that the degree of excitation-inhibition mismatch can be highly variable in individual neurons; some neurons receive only slightly mismatched excitation and inhibition, while others receive markedly mismatched excitation and inhibition. While excitatory input primarily determines where the BF is located, the inhibitory input can shift it and further enhance the difference in frequency preference between an individual neuron and the average of its local ensemble. Together, these effects provide a good explanation for the local heterogeneity of tuning properties; although adjacent neurons in both L4 and L5 all receive similar ranges of synaptic inputs as manifested by their similar subthreshold response areas (Figure S5, see also (Bandyopadhyay et al., 2010)), the detailed pattern of pairing between excitation and inhibition can be different, leading to the individualized shaping of frequency preference. Our results do not exclude the possibility that cell type differences also partially contribute to the functional diversity as more and more subtypes of pyramidal neurons are being identified (Aronoff et al., 2010; Harris and Shepherd, 2015; Hattox and Nelson, 2007; Poulin et al., 2016). However, it is still challenging to prudently identify the relationship between diverse functional properties and specific cell types. Instead, our results demonstrate a simple yet effective synaptic strategy to generate local tuning diversity. Whether this strategy can be applied to other cortical areas or layers where local functional diversity has been observed remains to be investigated.

Experimental Procedures

Animal preparation

All experimental procedures were approved by the Animal Care and Use Committee of Third Military Medical University. Experiments were conducted in a sound attenuation room. Adult Sprague-Dawley rats were used in this study. For awake state recording, the animal was anesthetized using isoflurane (1.5%). Several screws were fixed into the skull and a head fixation bar was glued on top of the skull using dental cement (Schwarz et al., 2010). The right auditory cortex was exposed, and the tonotopic gradients determined with extracellular recordings (Polley et al., 2007). After mapping, silicone elastomer was applied

to the opening for moisturization and protection. The animal was then habituated to be head-fixed, and ibuprofen and penicillin G was administered to the animal for three days. On the recording day, the rat was head-fixed using a customized apparatus and the body of the rat was restrained within a customized tube. Sugar water was delivered manually during the habituation and breaks of recording sessions. For in vivo recording in anesthetized state, the animal was anesthetized with urethane (1.5 g/kg).

Sound generation and calibration

A prepolarized condenser and a 1/4″ pressure microphone (Piezotronics Inc., USA) were used to calibrate the sound. The speaker (MF1, TDT Inc., USA) was driven by a stereo power amplifier (SA1, TDT Inc., USA). A high-speed DAQ board (National Instruments, USA) was used to record the sound. Customized LabVIEW programs were used to generate sound waveforms and perform calibration. To obtain TRFs, 568 pure tones (0.5 – 64 kHz, at 0.1-octave steps; 0 – 70 dB SPL, at 10 dB steps; 35 ms duration; 5 ms sine ramp; 250 ms interstimulus interval) were delivered to the left ear in pseudo-random order.

In vivo extracellular multiunit recording

Parylene-coated tungsten electrodes (100 kΩ, WPI Inc., USA) were used to record sound-evoked multiunit spikes. Signals were amplified and collected by TDT System 3 (TDT Inc., USA), and band-pass filtered (300/3000 Hz, High pass/Low pass).

In vivo patch-clamp recording

Cell-attached loose-patch recording—Experimental procedures were similar as we previously described (Tao et al., 2016; Tao et al., 2017). In brief, the same micromanipulator was used to hold the tungsten electrode and glass pipettes. To localize the glass pipette to the same site, we navigated the pipette under stereoscope (4X amplification) based on vasculature landmarks (Figure S2). Correct localization to the same place was evidenced by the matching of characteristic frequency between local field potential (LFP, recorded by the glass pipette) and multiunit (MUA, recorded by the tungsten electrode) responses. We directly compared the tracks of the tungsten electrode (coated with DiI, Thermo Fisher Scientific, USA) and glass pipette (coated with DiO, Thermo Fisher Scientific, USA) used in the same experiment (see Figure S2). The difference of penetration angle was small (1.5 ± 0.3°, n = 15 experiments). Given 800-μm travel distance, this can cause 21.2 ± 4.2 μm error in horizontal distance and negligible error in vertical distance (Figure S2E), which is acceptable for considering a local ensemble.

The pipette was filled with artificial cerebrospinal fluid (ACSF, in mM: 124 NaCl, 3 KCl, 1.23 NaH2PO4, 2.6 NaHCO3, 2 CaCl2, 10 glucose, 2 MgCl2, 2% biocytin, pH 7.25). A positive pressure (0.4 psi) was applied during cell hunting. When the pipette tip touched a neuron (indicated as an increase of the pipette impendence and spiny baseline), the pressure was released to form a loose seal. All the cells reported in this study were putative excitatory neurons (trough-to-peak interval > 0.4 ms) (Xiong et al., 2015; Zhou et al., 2010). 22 neurons were successfully reconstructed after biocytin-loading with electroporation (Joshi and Hawken, 2006; Tao et al., 2016). Neurons with raw TRF identifiable in each repetition, and PSTH with z-scores above 3 were considered as auditory responsive (Figure S6). To

obtain TRFs of nearby neurons, a mild positive pressure was reapplied after a previous recording. The pipette was vertically moved backward to the depth of 200 μm before starting the next cell hunting. Neurons located less than 100 μm apart were considered to be nearby cells. The depth of L4 cells ranged from 450 to 650 μm, and that of L5 cells ranged from 650 to 950 μm (Sun et al., 2013). We found that the cell depth based on travel distance was roughly in accordance with the depth determined after cell reconstruction (ΔD = − 4.1 ± 26.9 μm, mean ± SD, Figure S7).

Whole-Cell Recording—The procedure was similar as previously described (Tao et al., 2016). For in vivo current-clamp recordings, the internal solution contained (in mM): 4 MgATP, 125 K-gluconate, 0.3 GTP, 10 HEPES, 10 phosphocreatine, 1 EGTA, and 1% biocytin (pH 7.2). For sequential current clamp and voltage clamp recording, the solution contained (in mM): 5 TEA-Cl, 0.3 GTP, 125 Cs-gluconate, 10 phosphocreatine, 10 HEPES, 4 MgATP, 1 EGTA, 2 CsCl, 1% biocytin and 1.5 QX-314 (pH 7.2). The fast and slow capacitance were compensated completely, and the series resistance was compensated for 45%–50% to obtain an effective series resistance about 15–20 MΩ. The membrane potential was clamped at −70 mV and 0 mV for recording excitatory and inhibitory currents, respectively. The linear I-V relationship of the recorded synaptic currents (Figure S4) demonstrated that the quality of voltage clamp in our recordings was reasonably good (Tao et al., 2016; Zhou et al., 2010). The onsets of excitatory and inhibitory inputs were determined by the time point at which response amplitude exceeded the baseline by 3 standard deviations. Our whole-cell recording method biased towards excitatory pyramidal neurons as previously reported (Sun et al., 2010; Tao et al., 2016; Zhou et al., 2015).

Histology

After recording, the animals were deeply anesthetized and were transcardially perfused with saline and paraformaldehyde (PFA, 4% in phosphate-buffered saline, PBS). The brain was kept in PFA (4%) overnight and subsequently sliced at a thickness of 200 μm using a vibratome. The sections were incubated with an avidin–biotin HRP complex (ABC Kit, Vector Laboratories, Inc., USA) and then were moved into DAB solution (Vector® SG Substrate Kit, Vector Laboratories, Inc., USA). The imaging was obtained with a brightfield microscope (Nikon, Japen).

Retrograde Tracing

The rat was anesthetized using a mixture of ketamine (55mg/kg) and xylazine (6.4mg/kg). 0.5μl fluorescence-conjugated CTb (2.5% in PBS, ThermoFisher Scientific, Inc., USA) was injected into A1 and AAF at the depth of 450 μm using glass pipettes, at a rate of 40nl min-1. The pipette was withdrawn 10 min after injection. The animals were returned to their home cages and allowed to survive for at least 2 weeks before imaging (Olympus, Japan).

Data Analysis

The analyses of extracellular recording data were conducted online by using Brainware (TDT Inc., USA). The analyses of in vivo patch-clamp recording were performed offline using customized scripts in Matlab (MathWorks Inc., USA). Bandwidth was determined at each testing intensity by the number of tones between the “start” and “stop” points which

revoked responses with z-scores > 3, and the center was defined as the midpoint between the start and stop points. TRF size was then calculated as the sum of bandwidths at all intensities. Excitatory and inhibitory synaptic conductances were derived according to previous reports, based on the assumption that the recorded neuron was linear and isopotential (Tao et al., 2016):

$$I(t)=G_r(V_m(t)-V_{rest})+G_e(t)(V_m(t)-E_e)+G_i(t)(V_m(t)-E_i)$$

Vrest, resting membrane potential; I(t), amplitude of synaptic current at time point t; Gr, resting conductance; Vm, command voltage; Gi and Ge, the inhibitory and excitatory conductance; Ei (−70 mV) and Ee (0 mV), the reversal potentials for inhibition and excitation. We used a conductance-based neuron model to simulate the membrane potential response:

$$V_{t+1}=-\frac{dt}{C}[G_{e_t}(V_t-E_e)+G_{i_t}(V_t-E_i)+G_r(V_t-V_{rest})]+V_t$$

The values of C (100–150 pF) and Gr (15 nS) were based on measurements made during the experiments. The resting membrane potential (Vrest) was set to −70 mV.

Statistics

SPSS (IBM Inc., USA) was used for statistical analysis. For comparisons made between groups with statistically equal variances, t test or paired t-test was used. Welch *t* test was used to compare groups without equal variances. *F* test was applied to test variance equivalence. Shapiro–Wilk test was used to test the normality of data.

Supplementary Material

Refer to Web version on PubMed Central for supplementary material.

Acknowledgments

This work was supported by grants from National Natural Science Foundation of China (31271177, 31471056 and 31371116) L.I.Z. was supported by NIH R01DC008983. H.W.T. was supported by NIH R01EY019049.

References

Abeles M, Goldstein MH Jr. Functional architecture in cat primary auditory cortex: columnar organization and organization according to depth. J Neurophysiol. 1970; 33:172–187. [PubMed: 5411512]

Aronoff R, Matyas F, Mateo C, Ciron C, Schneider B, Petersen CC. Long-range connectivity of mouse primary somatosensory barrel cortex. Eur J Neurosci. 2010; 31:2221–2233. [PubMed: 20550566]

Bandyopadhyay S, Shamma SA, Kanold PO. Dichotomy of functional organization in the mouse auditory cortex. Nat Neurosci. 2010; 13:361–368. [PubMed: 20118924]

Callaway EM. Local circuits in primary visual cortex of the macaque monkey. Annu Rev Neurosci. 1998; 21:47–74. [PubMed: 9530491]

Dan Y, Poo MM. Spike timing-dependent plasticity: from synapse to perception. Physiol Rev. 2006; 86:1033–1048. [PubMed: 16816145]

Ehret, G., Romand, R. The central auditory system. New York: Oxford University Press; 1997.

Engert F, Tao HW, Zhang LI, Poo MM. Moving visual stimuli rapidly induce direction sensitivity of developing tectal neurons. Nature. 2002; 419:470–475. [PubMed: 12368854]

Fu YX, Shen Y, Gao H, Dan Y. Asymmetry in visual cortical circuits underlying motion-induced perceptual mislocalization. J Neurosci. 2004; 24:2165–2171. [PubMed: 14999067]

Guo W, Chambers AR, Darrow KN, Hancock KE, Shinn-Cunningham BG, Polley DB. Robustness of cortical topography across fields, laminae, anesthetic states, and neurophysiological signal types. J Neurosci. 2012; 32:9159–9172. [PubMed: 22764225]

Harris KD, Shepherd GM. The neocortical circuit: themes and variations. Nat Neurosci. 2015; 18:170–181. [PubMed: 25622573]

Hattox AM, Nelson SB. Layer V neurons in mouse cortex projecting to different targets have distinct physiological properties. J Neurophysiol. 2007; 98:3330–3340. [PubMed: 17898147]

Hromadka T, Deweese MR, Zador AM. Sparse representation of sounds in the unanesthetized auditory cortex. PLoS Biol. 2008; 6:e16. [PubMed: 18232737]

Intskirveli I, Joshi A, Vizcarra-Chacon BJ, Metherate R. Spectral breadth and laminar distribution of thalamocortical inputs to A1. J Neurophysiol. 2016; 115:2083–2094. [PubMed: 26888102]

Issa JB, Haeffele BD, Agarwal A, Bergles DE, Young ED, Yue DT. Multiscale optical Ca2+ imaging of tonal organization in mouse auditory cortex. Neuron. 2014; 83:944–959. [PubMed: 25088366]

Jiang X, Shen S, Cadwell CR, Berens P, Sinz F, Ecker AS, Patel S, Tolias AS. Principles of connectivity among morphologically defined cell types in adult neocortex. Science. 2015; 350:aac9462. [PubMed: 26612957]

Jiang X, Wang G, Lee AJ, Stornetta RL, Zhu JJ. The organization of two new cortical interneuronal circuits. Nat Neurosci. 2013; 16:210–218. [PubMed: 23313910]

Joshi S, Hawken MJ. Loose-patch-juxtacellular recording in vivo--a method for functional characterization and labeling of neurons in macaque V1. J Neurosci Methods. 2006; 156:37–49. [PubMed: 16540174]

Kanold PO, Nelken I, Polley DB. Local versus global scales of organization in auditory cortex. Trends Neurosci. 2014; 37:502–510. [PubMed: 25002236]

Kato HK, Gillet SN, Isaacson JS. Flexible Sensory Representations in Auditory Cortex Driven by Behavioral Relevance. Neuron. 2015; 88:1027–1039. [PubMed: 26586181]

Kerlin AM, Andermann ML, Berezovskii VK, Reid RC. Broadly tuned response properties of diverse inhibitory neuron subtypes in mouse visual cortex. Neuron. 2010; 67:858–871. [PubMed: 20826316]

Li LY, Ji XY, Liang F, Li YT, Xiao Z, Tao HW, Zhang LI. A feedforward inhibitory circuit mediates lateral refinement of sensory representation in upper layer 2/3 of mouse primary auditory cortex. J Neurosci. 2014; 34:13670–13683. [PubMed: 25297094]

Li LY, Li YT, Zhou M, Tao HW, Zhang LI. Intracortical multiplication of thalamocortical signals in mouse auditory cortex. Nat Neurosci. 2013a; 16:1179–1181. [PubMed: 23933752]

Li YT, Ibrahim LA, Liu BH, Zhang LI, Tao HW. Linear transformation of thalamocortical input by intracortical excitation. Nat Neurosci. 2013b; 16:1324–1330. [PubMed: 23933750]

Li YT, Liu BH, Chou XL, Zhang LI, Tao HW. Strengthening of Direction Selectivity by Broadly Tuned and Spatiotemporally Slightly Offset Inhibition in Mouse Visual Cortex. Cereb Cortex. 2015; 25:2466–2477. [PubMed: 24654259]

Lien AD, Scanziani M. Tuned thalamic excitation is amplified by visual cortical circuits. Nat Neurosci. 2013; 16:1315–1323. [PubMed: 23933748]

Lomber SG, Malhotra S. Double dissociation of ‘what’ and ‘where’ processing in auditory cortex. Nat Neurosci. 2008; 11:609–616. [PubMed: 18408717]

Maor I, Shalev A, Mizrahi A. Distinct Spatiotemporal Response Properties of Excitatory Versus Inhibitory Neurons in the Mouse Auditory Cortex. Cereb Cortex. 2016:4242–4252. [PubMed: 27600839]

Mehta MR, Quirk MC, Wilson MA. Experience-dependent asymmetric shape of hippocampal receptive fields. Neuron. 2000; 25:707–715. [PubMed: 10774737]

Merzenich MM, Knight PL, Roth GL. Representation of cochlea within primary auditory cortex in the cat. J Neurophysiol. 1975; 38:231–249. [PubMed: 1092814]

Morel A, Imig TJ. Thalamic projections to fields A, AI, P, and VP in the cat auditory cortex. J Comp Neurol. 1987; 265:119–144. [PubMed: 2826552]

Ohki K, Chung S, Ch'ng YH, Kara P, Reid RC. Functional imaging with cellular resolution reveals precise micro-architecture in visual cortex. Nature. 2005; 433:597–603. [PubMed: 15660108]

Polley DB, Read HL, Storace DA, Merzenich MM. Multiparametric auditory receptive field organization across five cortical fields in the albino rat. J Neurophysiol. 2007; 97:3621–3638. [PubMed: 17376842]

Poulin JF, Tasic B, Hjerling-Leffler J, Trimarchi JM, Awatramani R. Disentangling neural cell diversity using single-cell transcriptomics. Nat Neurosci. 2016; 19:1131–1141. [PubMed: 27571192]

Read HL, Winer JA, Schreiner CE. Functional architecture of auditory cortex. Curr Opin Neurobiol. 2002; 12:433–440. [PubMed: 12139992]

Rothschild G, Mizrahi A. Global order and local disorder in brain maps. Annu Rev Neurosci. 2015; 38:247–268. [PubMed: 25897872]

Rothschild G, Nelken I, Mizrahi A. Functional organization and population dynamics in the mouse primary auditory cortex. Nat Neurosci. 2010; 13:353–360. [PubMed: 20118927]

Sadagopan S, Wang X. Level invariant representation of sounds by populations of neurons in primary auditory cortex. J Neurosci. 2008; 28:3415–3426. [PubMed: 18367608]

Sakata S, Harris KD. Laminar structure of spontaneous and sensory-evoked population activity in auditory cortex. Neuron. 2009; 64:404–418. [PubMed: 19914188]

Schreiner CE, Read HL, Sutter ML. Modular organization of frequency integration in primary auditory cortex. Annu Rev Neurosci. 2000; 23:501–529. [PubMed: 10845073]

Schreiner CE, Sutter ML. Topography of excitatory bandwidth in cat primary auditory cortex: single-neuron versus multiple-neuron recordings. J Neurophysiol. 1992; 68:1487–1502. [PubMed: 1479426]

Schwarz C, Hentschke H, Butovas S, Haiss F, Stuttgen MC, Gerdjikov TV, Bergner CG, Waiblinger C. The head-fixed behaving rat--procedures and pitfalls. Somatosens Mot Res. 2010; 27:131–148. [PubMed: 20954892]

Smith SL, Hausser M. Parallel processing of visual space by neighboring neurons in mouse visual cortex. Nat Neurosci. 2010; 13:1144–1149. [PubMed: 20711183]

South DA, Weinberger NM. A comparison of tone-evoked response properties of 'cluster' recordings and their constituent single cells in the auditory cortex. Brain Res. 1995; 704:275–288. [PubMed: 8788924]

Stettler DD, Axel R. Representations of odor in the piriform cortex. Neuron. 2009; 63:854–864. [PubMed: 19778513]

Sugimoto S, Sakurada M, Horikawa J, Taniguchi I. The columnar and layer-specific response properties of neurons in the primary auditory cortex of Mongolian gerbils. Hear Res. 1997; 112:175–185. [PubMed: 9367240]

Sun W, Tan Z, Mensh BD, Ji N. Thalamus provides layer 4 of primary visual cortex with orientation- and direction-tuned inputs. Nat Neurosci. 2016; 19:308–315. [PubMed: 26691829]

Sun YJ, Kim YJ, Ibrahim LA, Tao HW, Zhang LI. Synaptic mechanisms underlying functional dichotomy between intrinsic-bursting and regular-spiking neurons in auditory cortical layer 5. J Neurosci. 2013; 33:5326–5339. [PubMed: 23516297]

Sun YJ, Wu GK, Liu BH, Li P, Zhou M, Xiao Z, Tao HW, Zhang LI. Fine-tuning of pre-balanced excitation and inhibition during auditory cortical development. Nature. 2010; 465:927–931. [PubMed: 20559386]

Szymanski FD, Garcia-Lazaro JA, Schnupp JW. Current source density profiles of stimulus-specific adaptation in rat auditory cortex. J Neurophysiol. 2009; 102:1483–1490. [PubMed: 19571199]

Tao C, Zhang G, Zhou C, Wang L, Yan S, Zhang LI, Zhou Y, Xiong Y. Synaptic Basis for the Generation of Response Variation in Auditory Cortex. Sci Rep. 2016; 6:31024. [PubMed: 27484928]

Tao C, Zhang G, Zhou C, Wang L, Yan S, zhou Y, Xiong Y. Bidirectional Shifting Effects of the Sound Intensity on the Best Frequency in the Rat Auditory Cortex. Sci Rep. 2017; 7:44493. [PubMed: 28290533]

Wallace MN, Palmer AR. Laminar differences in the response properties of cells in the primary auditory cortex. Exp Brain Res. 2008; 184:179–191. [PubMed: 17828392]

Wehr M, Zador AM. Balanced inhibition underlies tuning and sharpens spike timing in auditory cortex. Nature. 2003; 426:442–446. [PubMed: 14647382]

Winkowski DE, Kanold PO. Laminar transformation of frequency organization in auditory cortex. J Neurosci. 2013; 33:1498–1508. [PubMed: 23345224]

Woodin MA, Ganguly K, Poo MM. Coincident pre- and postsynaptic activity modifies GABAergic synapses by postsynaptic changes in Cl-transporter activity. Neuron. 2003; 39:807–820. [PubMed: 12948447]

Wu GK, Arbuckle R, Liu BH, Tao HW, Zhang LI. Lateral sharpening of cortical frequency tuning by approximately balanced inhibition. Neuron. 2008; 58:132–143. [PubMed: 18400169]

Wu GK, Li P, Tao HW, Zhang LI. Nonmonotonic synaptic excitation and imbalanced inhibition underlying cortical intensity tuning. Neuron. 2006; 52:705–715. [PubMed: 17114053]

Wu GK, Tao HW, Zhang LI. From elementary synaptic circuits to information processing in primary auditory cortex. Neurosci Biobehav Rev. 2011; 35:2094–2104. [PubMed: 21609731]

Xiong XR, Liang F, Zingg B, Ji XY, Ibrahim LA, Tao HW, Zhang LI. Auditory cortex controls sound-driven innate defense behaviour through corticofugal projections to inferior colliculus. Nat Commun. 2015; 6:7224. [PubMed: 26068082]

Zhang LI, Bao S, Merzenich MM. Persistent and specific influences of early acoustic environments on primary auditory cortex. Nat Neurosci. 2001; 4:1123–1130. [PubMed: 11687817]

Zhang LI, Tan AY, Schreiner CE, Merzenich MM. Topography and synaptic shaping of direction selectivity in primary auditory cortex. Nature. 2003; 424:201–205. [PubMed: 12853959]

Zhou M, Li YT, Yuan W, Tao HW, Zhang LI. Synaptic mechanisms for generating temporal diversity of auditory representation in the dorsal cochlear nucleus. J Neurophysiol. 2015; 113:1358–1368. [PubMed: 25475349]

Zhou Y, Liu BH, Wu GK, Kim YJ, Xiao Z, Tao HW, Zhang LI. Preceding inhibition silences layer 6 neurons in auditory cortex. Neuron. 2010; 65:706–717. [PubMed: 20223205]

Znamenskiy P, Zador AM. Corticostriatal neurons in auditory cortex drive decisions during auditory discrimination. Nature. 2013; 497:482–485. [PubMed: 23636333]

Highlights

1. Layer 5 neurons in the anterior auditory field show local functional heterogeneity.
2. Tuning profiles of synaptic excitation and inhibition are diversely mismatched.
3. Diversely skewed excitation primarily determines this mismatch.
4. Symmetric inhibition enhances the local functional diversity.

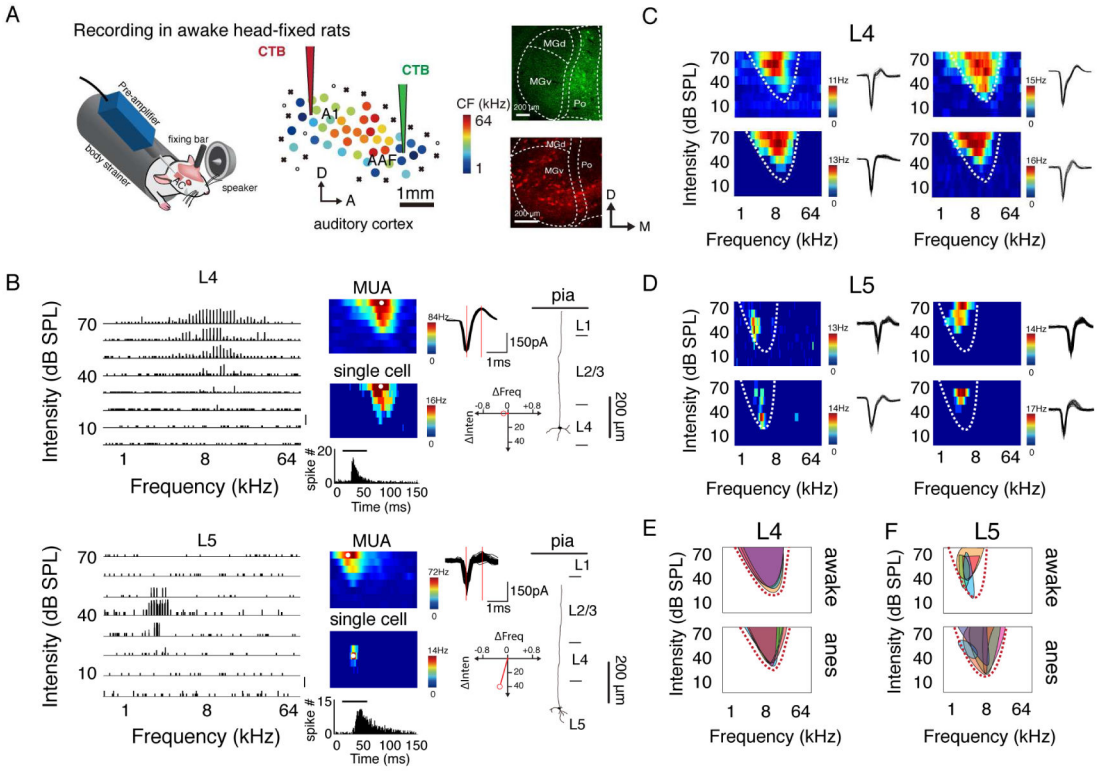

Figure 1. TRFs of single neurons in L5 of AAF differ from those of MUA

(A) Left, recording setup. Middle, an example mapping of auditory cortex. Color of each dot represents its characteristic frequency (CF). A1, primary auditory cortex; AAF, anterior auditory field; A, anterior; D, dorsal. “x” indicates a site with no detectable multiunit responses to sounds lower than 70 dB SPL. “o” indicates a site that does not show clear frequency tuning but has responses to noise at ≥ 60 dB SPL. Right, retrograde labelling in the thalamus by injecting red and green CTB tracers in the lower frequency regions of A1 and AAF, respectively. (B) Example reconstructed spike TRFs of neurons in L4 and L5 of AAF, which are plotted as an array of PSTHs for the responses to pure tones of different frequency-intensity combinations. Each PSTH trace represents the tone-evoked spike response averaged over 5 repetitions. Bin size, 10 ms. Scale, 0.5 spike count. Middle, color maps represent TRFs of average evoked spiking rate over 3 trials for MUA (upper) and over 5 trials for a single neuron (middle) at the same cortical location. Bottom inset, PSTH generated from the spike responses to all effective tones; the bar represents the duration of tone stimuli. Right, 50 superimposed randomly selected spike waveforms of the neuron with the red vertical lines marking the trough-to-peak interval (upper); red vector depicting the difference in stimulus preference between a single neuron and MUA (lower); reconstructed morphology of the recorded neuron. (C, D) Spike TRFs of four adjacent neurons in L4 (C) and L5 (D). Color map represents averaged spiking rate. Spike waveforms are shown to the right. Dashed curves outline the TRF of MUA at the same location. (E, F) Superimposed spike TRFs of adjacent neurons. Each shaded region represents the TRF of one individual neuron. Top, awake state; bottom, anesthetized state. Dashed curves outline the TRF of MUA at the cortical location.

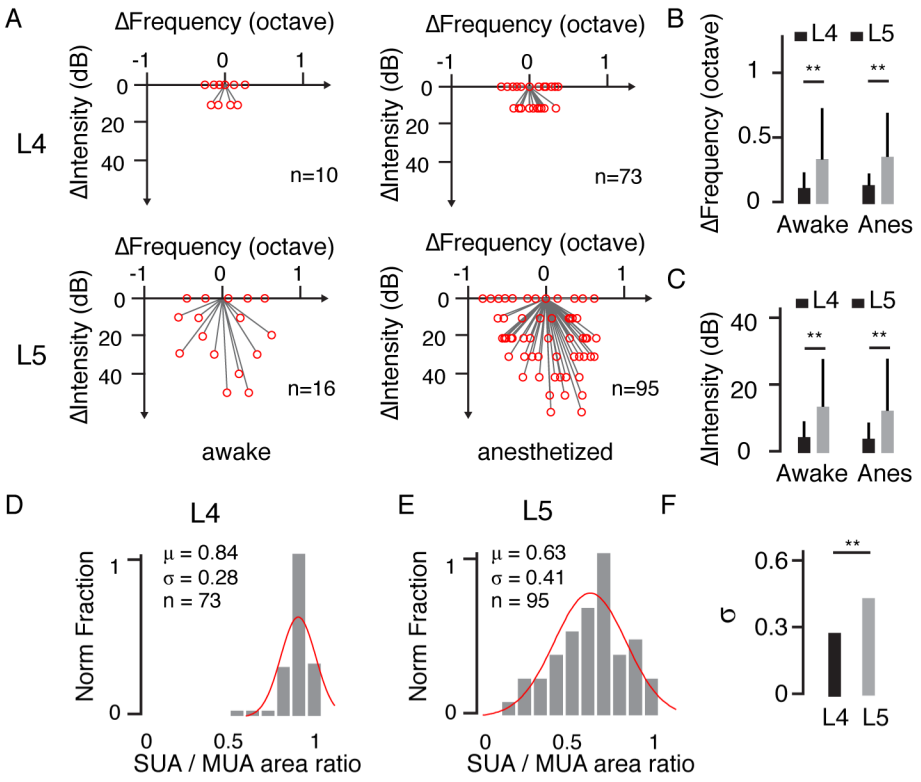

Figure 2. Diverse stimulus preferences of local L5 neurons

(A) Difference in stimulus preference between a single neuron and the corresponding MUA. Left, awake condition (L4, n = 10; L5, n = 16); right, anesthetized condition (L4, n = 73; L5, n = 95). (B, C) Difference in preferred frequency and preferred intensity between a single neuron (SUA) and its corresponding MUA. **, $p < 0.01$, Welch *t* test. (D, E) Normalized distribution of TRF size ratio between SUA and MUA in the anesthetized state. Red curve, fitting with a normal distribution. (F) Comparison of the broadness of the distribution between L4 and L5. **, $p < 0.01$, *F* test of equality of variances.

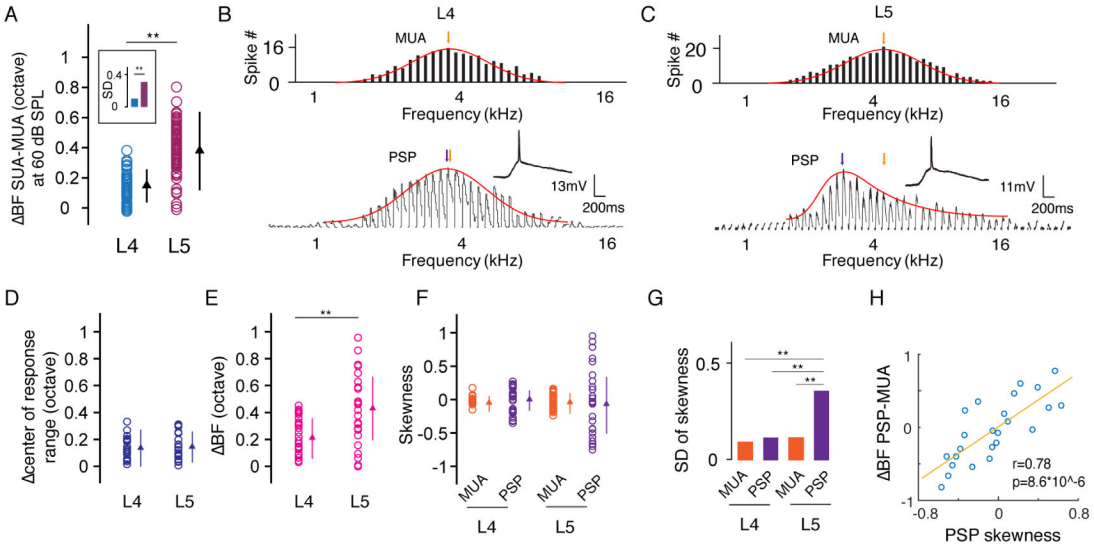

Figure 3. Diversity of membrane potential response tuning

(A) Difference in BF between SUA and MUA quantified at 60 dB SPL (L4, n = 20; L5, n = 24). **, $p < 0.01$, Welch *t* test. The comparison of SD is boxed, **, $p < 0.01$, *F* test. (B, C) Comparison of frequency tuning between MUA (upper) and postsynaptic potential (PSP, after filtering out spikes) of a single neuron (lower) at 60 dB SPL. Red curve, fitting with normal or skew normal distribution. The colored arrow points to the BF. (D) Difference in the response range center between MUA and PSP. **, $p = 0.51$, *t* test. Bar = SD. (E) Difference in BF between MUA and PSP. **, $p < 0.01$, *t* test. Bar = SD. (F) Skewness of MUA and PSP tuning. Bar = SD. (G) SD of the skewness values of MUA and PSP tuning. **, $p < 0.01$, *F* test. (H) Difference in BF between PSP and MUA plotted against the skewness of PSP tuning.

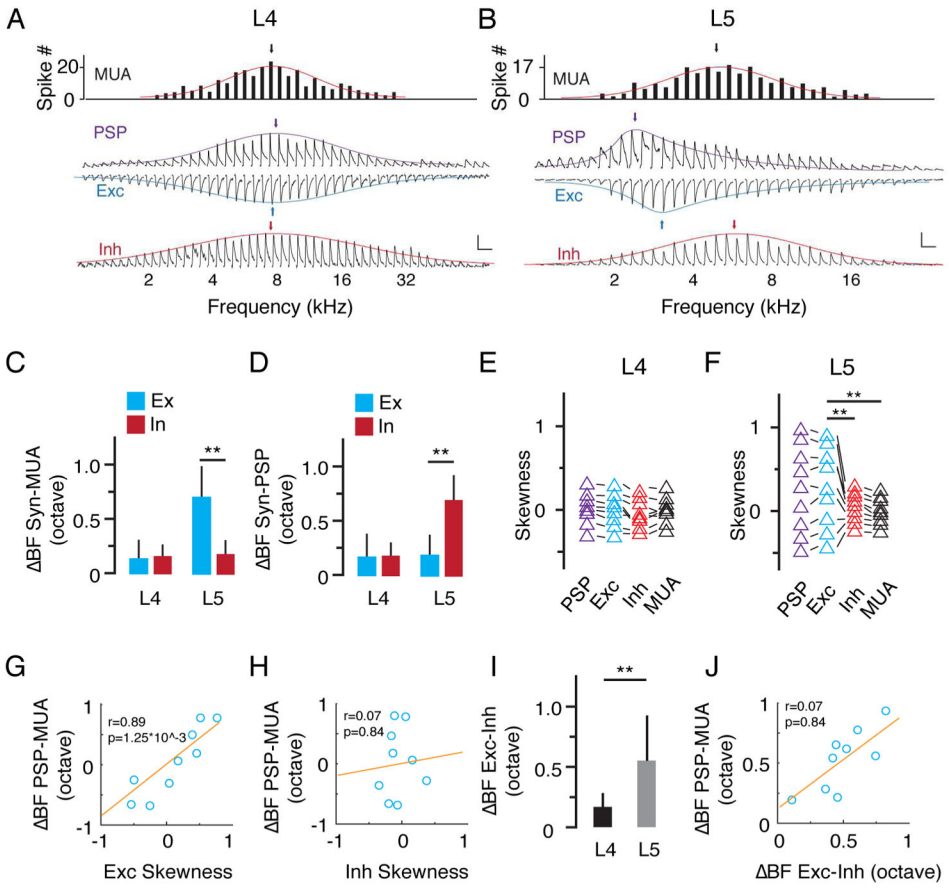

Figure 4. Skewed excitatory inputs dominantly contribute to the tuning diversity in L5

(A, B) Tuning curves of MUA, PSP, excitation and inhibition at 60 dB SPL for an example neuron. The colored curves are fitted normal or skew normal distribution functions. The arrow points to the BF. Scale: 10 mV for PSP; 200 pA for Exc; 150 pA for Inh, 200 ms for all. (C) Difference in BF between synaptic input and MUA. Blue, excitation; red, inhibition. **, $p < 0.01$, Welch *t* test. (D) Difference in BF between synaptic input and PSP. **, $p < 0.01$, Welch *t* test. (E) Skewness of PSP, excitation, inhibition and MUA tuning in L4 neurons. Data points obtained from the same neuron were connected with lines. (F) Skewness of PSP, excitation, inhibition and MUA tuning in L5. **, $p < 0.01$, F test. (G) Difference in BF between PSP and MUA plotted against the skewness of excitatory tuning. Red line is the best-fit linear regression line. (H) Difference in BF between PSP and MUA plotted against the skewness of inhibitory tuning. (I) Difference in BF between excitation and inhibition (absolute value) in L4 and L5, **, $p < 0.01$, Welch *t* test. (J) Difference in BF between PSP and MUA plotted against that between excitation and inhibition.

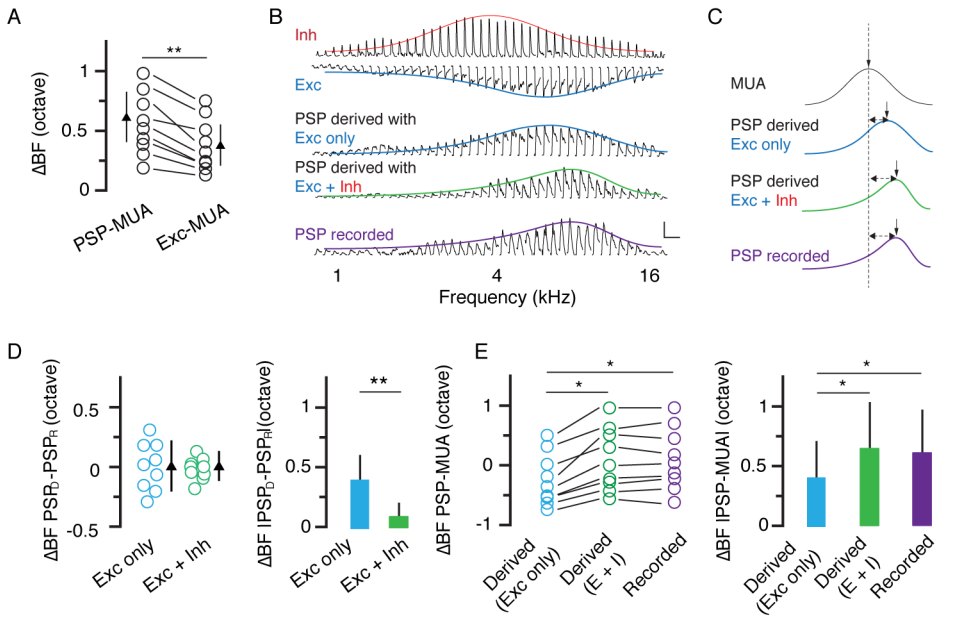

Figure 5. Inhibition expands tuning diversity in L5

(A) Difference in BF between PSP and MUA and that between excitation and MUA. **, $p < 0.01$, paired *t* test. (B) Tuning curves of inhibition, excitation, PSP derived from excitation only, PSP derived from the integration of excitation and inhibition, and recorded PSP for an example L5 neuron. Scale: 10 mV and 200 ms. (C) Comparison of fitted normal or skew normal distribution curves of the same cell in (B). The vertical arrow points to the BF. The dashed line marks the BF of MUA. (D) Difference in BF between derived PSP and recorded PSP. Bar = SD. Right, same data but in absolute value. **, $p < 0.01$, paired *t* test. (E) Difference in BF between PSP (derived or recorded) and MUA. Data points obtained from the same neuron are connected with lines. *, $p < 0.05$, one-way ANOVA, post hoc test. Right, same data but in absolute value. *, $p < 0.05$, one-way ANOVA, post hoc test.

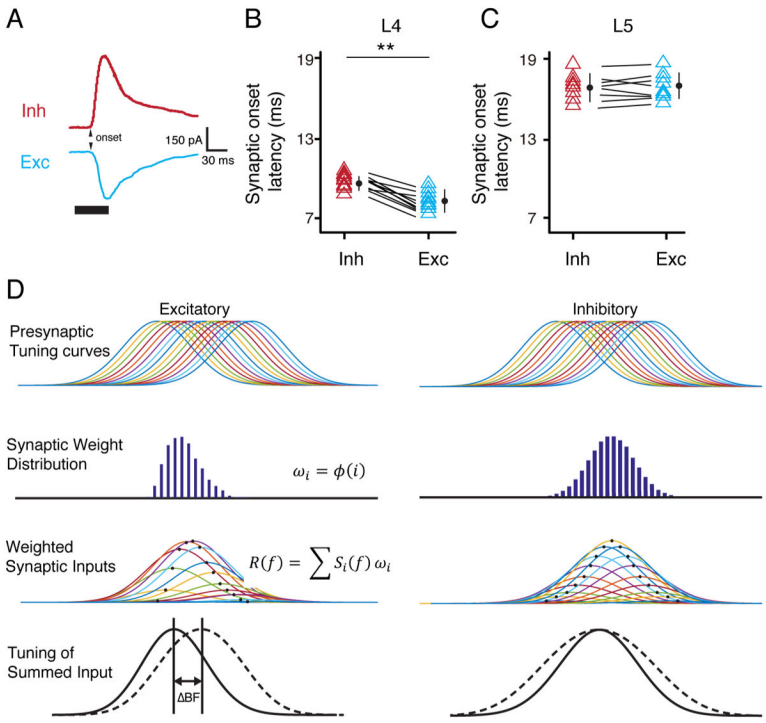

Figure 6. Onset latencies of synaptic inputs to L5 neurons and a proposed model

(A) Average recorded synaptic responses to BF tone in an example L5 neuron. Inh, inhibition; Exc, excitation. Arrow points to the synaptic onset. (B, C) Synaptic onset latencies of excitation and inhibition in L4 and L5 neurons. **, $p < 0.01$, paired *t* test. Bar = SD. (D) First row, symmetric tuning curves of output responses of a series of presynaptic (excitatory and inhibitory) neurons for an L5 cell. Second row, distribution of synaptic weights of the inputs, which is asymmetric for excitatory inputs but symmetric for inhibitory inputs. Third row, tuning curves of weighted synaptic inputs (output times synaptic weight). Fourth row, summing up the individual curves of weighted synaptic input (solid curve) produces asymmetric excitatory tuning and symmetric inhibitory tuning. The dashed curve represents the sum of synaptic inputs of equal strengths.